RSC Advances

PAPER

View Article Online
View Journal | View Issue

Cite this: *RSC Adv.*, 2020, **10**, 38890

Wide bandgap semiconductor-based novel nanohybrid for potential antibacterial activity: ultrafast spectroscopy and computational studies

Md. Nur Hasan,[a] Tuhin Kumar Maji,[a] Uttam Pal,[b] Arpan Bera,[a] Damayanti Bagchi,[a] Animesh Halder,[bc] Saleh A. Ahmed,[de] Jabir H. Al-Fahemi,[d] Tahani M. Bawazeer,[d] Tanusri Saha-Dasgupta[bfg] and Samir Kumar Pal[*ab]

The properties of nanomaterials generated by external stimuli are considered an innovative and promising replacement for the annihilation of bacterial infectious diseases. The present study demonstrates the possibility of getting the antibiotic-like drug action from our newly synthesized nanohybrid (NH), which consists of norfloxacin (NF) as the photosensitive material covalently attached to the ZnO nanoparticle (NP). The synthesized NH has been characterized using various microscopic and spectroscopic techniques. Steady state fluorescence and time-correlated single photon counting (TCSPC)-based spectroscopic studies demonstrate the efficient electron transfer from NF to ZnO. This enhances the reactive oxygen species (ROS) production capability of the system. First principles density functional theory has been calculated to gain insight into the charge separation mechanism. To explore the electron densities of the occupied and unoccupied levels of NH, we have verified the nature of the electronic structure. It is observed that there is a very high possibility of electron transfer from NF to ZnO in the NH system, which validates the experimental findings. Finally, the efficacy of NH compared to NF and ZnO has been estimated on the *in vitro* culture of *E. coli* bacteria. We have obtained a significant reduction in the bacterial viability by NH with respect to control in the presence of light. These results suggest that the synthesized NH could be a potential candidate in the new generation alternative antibacterial drugs. Overall, the study depicts a detailed physical insight for nanohybrid systems that can be beneficial for manifold application purposes.

Received 30th August 2020
Accepted 5th October 2020

DOI: 10.1039/d0ra07441a

rsc.li/rsc-advances

1. Introduction

Bacterial infections are one of the most dangerous health problems worldwide that affect almost all age groups of people,[1] and initiate various social and economic complications.[2,3] Increased infections and outbreaks related to pathogenic burden, antibiotic infection of bacteria, the emergence of new bacterial mutations, and shortage of applicable vaccines create danger for people's health worldwide, especially in children.[4] These are most generally treated by broad-spectrum antibiotics (such as norfloxacin, ciprofloxacin, tetracyclin, and meticillin).[5] However, they have some limitations, such as the overuse of antibiotics, extended durations of treatment, use of subtherapeutic dosages, prophylactic use of antibiotics, and misuse of antibiotics for other non-bacterial infections.[1,6,7] So, it is necessary to develop a new alternative strategy (targeted and stimuli-responsive) to overcome bacterial infections.

The implementation of light harvesting nanomaterials (such as metallic and inorganic oxide nanoparticles) for numerous targeted biomedical aspects is presently going through a dramatic expansion.[8,9] In the last few years, photosensitizers (PS) have been broadly used in antibacterial photodynamic therapy (PDT) because of the high molar extinction coefficient, less toxicity, and good biocompatibility.[10,11] Some reports on their photocatalytic activity are also present.[12] They can generate reactive oxygen species (ROS) from neighboring water and oxygen molecules upon excitation.[13] These ROS are responsible for their antibacterial, antifungal, and anticancer activity.[14] However, there are some limitations associated with photosensitizers that restrict their practical applications.[15] Many PS

[a]*Department of Chemical, Biological & Macromolecular Sciences, S. N. Bose National Centre for Basic Sciences, Block JD, Sector-III, Salt Lake, Kolkata 700106, India. E-mail: skpal@bose.res.in*

[b]*Technical Research Centre, S. N. Bose National Centre for Basic Sciences, Block JD, Sector-III, Salt Lake, Kolkata 700106, India*

[c]*Department of Applied Optics & Photonics, University of Calcutta, Block JD, Sector-III, Salt Lake, Kolkata 700106, India*

[d]*Chemistry Department, Faculty of Applied Sciences, Umm Al-Qura University, 21955 Makkah, Saudi Arabia*

[e]*Chemistry Department, Faculty of Science, Assiut University, 71516 Assiut, Egypt*

[f]*Department of Condensed Matter Physics and Material Sciences, S. N. Bose National Centre for Basic Sciences, Block JD, Sector-III, Salt Lake, Kolkata 700106, India*

[g]*School of Mathematical & Computational Sciences, Indian Association for the Cultivation of Science, Raja S. C. Mullick Road, Kolkata 700032, India*

have poor solubility in polar protic solvents (many dyes undergo aggregation in polar protic solvents), very short circulation time and poor photostability.[16,17] In order to avoid these limitations for both photosensitizers and inorganic nanoparticles, the formulation of an organic–inorganic (unit cell to large crystal) nanohybrid (NH) is of great importance in this field.[18]

There is a high demand for the development of stimuli-sensible NH just because of multifunction, multiuse and highly effective implementation.[19,20] Nowadays, nanoparticles (NPs) are increasingly used to target bacteria and could serve as an alternative to organic antibacterial agents.[21,22] The efficacy of antibacterial agents may be increased *via* nano-binding that could be effective to obstruct infections in humans, animals, as well as prevent the growth of bacteria in family products.[23] The NH is likely to remain safe against degradation, developing bioavailability, and advancement in intracellular penetration, controlled delivery of the drug and enhanced efficacy.[24–27] Therefore, the improvement of new antibiotics is a necessary thing to constantly achieve, but this kind of attempt has already passed since the late 1980s just because of the relatively low potential recovery on the investment and high expenditure of development.[28] Hence, our attention has been focused on newly synthesized, less toxic, low cost and exciting NP-based light harvesting hybrid materials with antibacterial activity.

The inappropriate and inconsistent use of these antibacterial agents gives rise to unwholesome or harmful bacteria.[29] Thus, improving the novel, light sensitive antibacterial drugs against bacterial strains, most primary food pathogens, like *Escherichia coli*, *Staphylococcus aureus*, *Salmonella typhi*, and *Clostridium perfringens*, has become the ultimate challenge.[30] The potential toxicology of the newly synthesized hybrid materials upon light exposure is mysterious.[31] Such kinds of medication could be applied to the affected tissue, while the surrounding cells remain normal, active, healthy and unhurt.[32] This requires the drugs or NH materials to be activated in the targeted organism. Recently, nanotechnology and NP-based materials have adopted important attention in antibiotics, antimicrobial action against bacteria, and more specifically for cancer therapy.[33]

In our present study, we report a new approach that focuses on a very well known antibiotic, norfloxacin (NF). NF has been widely used in the medicinal sector for varicose disease, including urinary tract infection in chronically catheterized patients.[34,35] We chose a wide bandgap semiconductor ZnO NP due to its advantages (compared to other NPs, such as targeted delivery vehicles, non-toxic, chemically reliable, biodegradable, excellent wide bandgap, greater binding energy (60 MeV), lower cost and abundance in nature[32,36–38]) and developed two different sizes of NF-functionalized nanohybrids (NHs) using ZnO NP (~5 nm and ~30 nm) to study the effect of crystal dimension on molecular interaction in NH. We have chosen the fluorescence properties of 5 nm ZnO NPs to confirm the NH formation and excited state electron transfer dynamics from ZnO to NF. As 5 nm ZnO is not stable at room temperature, we have used 30 nm ZnO for application purposes. The newly synthesized NH has been characterized using various microscopic and spectroscopic techniques. We have characterized the inorganic crystal of the synthesized nanohybrid with high-resolution electron microscopy (HRTEM) and X-ray diffraction technique (XRD). To represent the optical spectroscopy properties of the systems, UV-Visible spectroscopy was used. Steady-state fluorescence and picosecond resolved time correlated single photon counting (TCSPC) spectroscopy studies demonstrate the efficient electron transfer from NF to ZnO NP. This enhances the reactive oxygen species (ROS) generation capability of the system. First principles density functional theory (DFT) calculation has been operated using the Vienna *ab initio* simulation package (VASP) code to understand the charge separation mechanism of both unit cell ZnO and bulk ZnO complexes. To explore the electron densities of the occupied and unoccupied levels of the ZnO–NF complex, we have investigated the nature of the electronic structure for both complexes. It is observed that there is a high chance of charge transfer from NF to ZnO in both NH systems, which validates the experimental findings. Finally, for the potential applications of the NH system, an *in vitro* bacteria culture has been performed on *E. coli* bacteria, where we observed a significant bacterial death by the complex, compared to the free NF in the presence of UV light at 375 nm wavelength. These results suggest that the synthesized NH can be a potential candidate in the new generation antibacterial PDTs (Scheme 1).

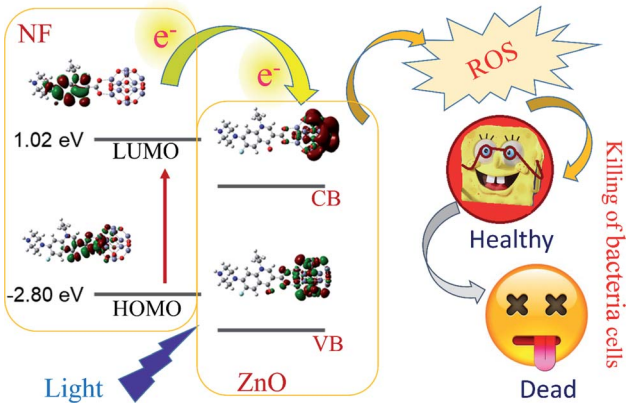

Scheme 1 Schematic representation of electron shuttling in the semiconductor ZnO nanostructure, leading to antibacterial activity.

2. Experimental section

2.1. Reagents

In our overall study, all of the chemicals were of analytical grade. The chemicals were used beyond any further purification. Sodium dihydrogen phosphate (NaH_2PO_4) and sodium hydroxide (NaOH) were obtained from Merck. The zinc acetate dihydrate ($(CH_3COO)_2Zn\cdot 2H_2O$) and dichlorofluorescin diacetate (DCFH-DA) were obtained from Sigma Aldrich. ZnO nanoparticles (approximately 30 nm), NF and ethanol were purchased from Sigma Aldrich. Dimethyl sulfoxide (DMSO) was purchased from Merck. The double-distilled water from a Millipore system (18.2 MΩ cm) was used in our present study.

2.2. Synthesis of 5 nm ZnO NPs

ZnO NPs of size 5 nm were prepared in aqueous ethanolic medium following a method as described in ref. 39. 20 mL 4 mM $(CH_3COO)_2Zn\cdot 2H_2O$ was heated at 60 °C for 30 min. 20 mL 4 mM NaOH in ethanol was added to this solution. The mixture was vigorously stirred for 2 h at around 60 °C. The resulting ZnO NPs solution was cooled down to room temperature, and then reserved at 4 °C until further need.

2.3. Preparation of nanohybrids

The surface of 30 nm ZnO NPs were functionalized by NF by adding 15 mg of 30 nm ZnO NPs to 15 mL of NF solution (0.25 mM solution in DMSO) with regular stirring at room temperature for 15 h. After 15 h, the solution was then centrifuged for 30 min. Then, the NH was washed with DMSO three times to remove free dyes. After washing, the NH was then dried in an oven for 8 h under 140 °C. Similarly, the surface of ~5 nm ZnO NPs were functionalized by NF by adding 15 mL of ZnO (5 nm) NPs to 15 mL of the NF solution (0.25 mM solution in ethanol) with continuous stirring at room temperature for 15 h, followed by washing. The final solution was taken at 4 °C until further use.

2.4. Characterization methods

The TEM grids of the NH microsphere were prepared by putting a diluted drop of the sample to carbon-coated copper grids. The size of the particles was analyzed from micrographs at a magnification of 100 000× using an FEI (Technai S-Twin, operating at 200 kV) instrument. The XRD pattern was carried out in the range from 10° to 80° using a PANalytical XPERTPRO diffractometer to characterize the crystal phase. A Shimadzu UV-2600 (spectrophotometer) was used to measure the absorption spectra of ZnO, NF, and NH using a 1 cm path quartz cell. A Jobin Yvon Fluorolog was used for the measurement of the room temperature emission spectra and excitation spectra. Time resolved spectroscopic studies were performed using a TCSPC setup from Edinburgh Instruments, with an instrument response function (IRF) of 82 ps upon excitation with 375 nm laser light and monitoring at 440 nm.

2.5. *In vitro* measurement of ROS

ROS creation ability for all samples was checked using dichlorofluorescin (DCFH) following a reported method.[40,41] DCFH was synthesized from commercial DCFH-DA. 1.0 mM DCFH-DA in 0.5 mL methanol was mixed with 2.0 mL, 0.01 M NaOH at room temperature up to around 30 min. 10 mL, 25 mM NaH_2PO_4 was used to neutralize the solution. We used NF (0.5 μM), the ZnO–NF nanohybrid (the concentration of NF in the nanohybrid is 0.5 μM), and 30 nm ZnO (maintaining the O.D. at 369 nm, similar to the ZnO–NF nanohybrid, which contains 0.5 μM of NF) for ROS measurement. The experiments were performed in a total time of 40 minutes (initial 15 minutes under dark, and then up to 25 minutes under irradiation of UV light of wavelength 375 nm).

2.6. Bacterial culture condition

The antibacterial culture was performed with *E. coli* cells, following a reported method.[42] To observe the bacterial growth analysis under different treatment conditions, bacterial cells were cultured at 37 °C in a Luria Broth (LB) medium for 12 h. It was then diluted 1000 times, and different samples were added. The bacterial assay experiment was cultured in different cuvettes containing 30 nm ZnO nanohybrids (0.5 mg mL^{-1} sample of nanohybrids, which contains 0.5 μM NF), 30 nm ZnO NPs (maintaining the O.D. at 369 nm, similar to the 30 nm ZnO nanohybrid), NF (concentration of NF used on the basis of NF loading on the surface of ZnO NPs) and DMSO. The samples were incubated at 37 °C after irradiation of UV light (wavelength 375 nm) for 30 minutes. In order to verify the reduction effect of the drugs, the absorbance was taken every hour and it was repeated for up to ~25 h. Finally, the absorbance of all samples was performed and plotted with respect to time. The nature of the plot suggests the relative effectiveness of the ZnO–NF samples as antibacterial drugs.

3. Computational methods

We used the VASP, adopting Generalized Gradient Approximation (GGA) and Projector Augmented Wave (PAW) schemes.[43–45] The *k*-points were chosen by using the Monkhorst–Pack method,[46] and typical values of the *k*-point mesh were (2 × 2 × 1), where 1 corresponds to the elongated direction of the supercell. The detailed calculation process is followed by our earlier work.[47] The unit cell of the ZnO wurtzite structure with 8 atoms was pre-optimized with a *k*-point density of 11 × 11 × 11. Supercells were built by repeating the optimized unit cell. For the simulation of the surface, the periodically repeating slab geometry was employed. Each slab was separated by the vacuum. For the $[10\bar{1}0]$ and [0001] surfaces (non-polar zig-zag end and polar Zn end, respectively), there were 120 Zn and 120 O arranged in 8 layers. For the $[11\bar{2}0]$ surface (non-polar arm-chair end), there were 108 Zn and 108 O arranged in 6 layers. NF was attached to the surface with various orientations, assuming bidentate attachment through the carboxylic and carbonyl O of NF with Zn.

4. Results and discussions

4.1. Structural characterization

Fig. 1(a) depicts the structure of NF. It has a carboxylic (–COOH) group, which can form a bond with another material. The powder X-ray diffraction (XRD) of the ZnO nanoparticles displayed many peaks, which indicates the presence of many diffraction planes. The XRD patterns of ZnO (Blue) and NF–ZnO (Red) are depicted in Fig. 1(b). The diffraction peaks are well-indexed using JCPDS Card No. 36-1451, which confirms the wurtzite ZnO. No additional peaks were obtained in the X-ray diffraction patterns, which proposed its crystalline impurities. NH shows the same nature of the diffraction peaks as ZnO, which confirms that there is no change of phase during the formation of NH. The crystalline nature and size of the synthesized ~5 nm ZnO NP, ~30 nm ZnO NP, ~5 nm ZnO–NF

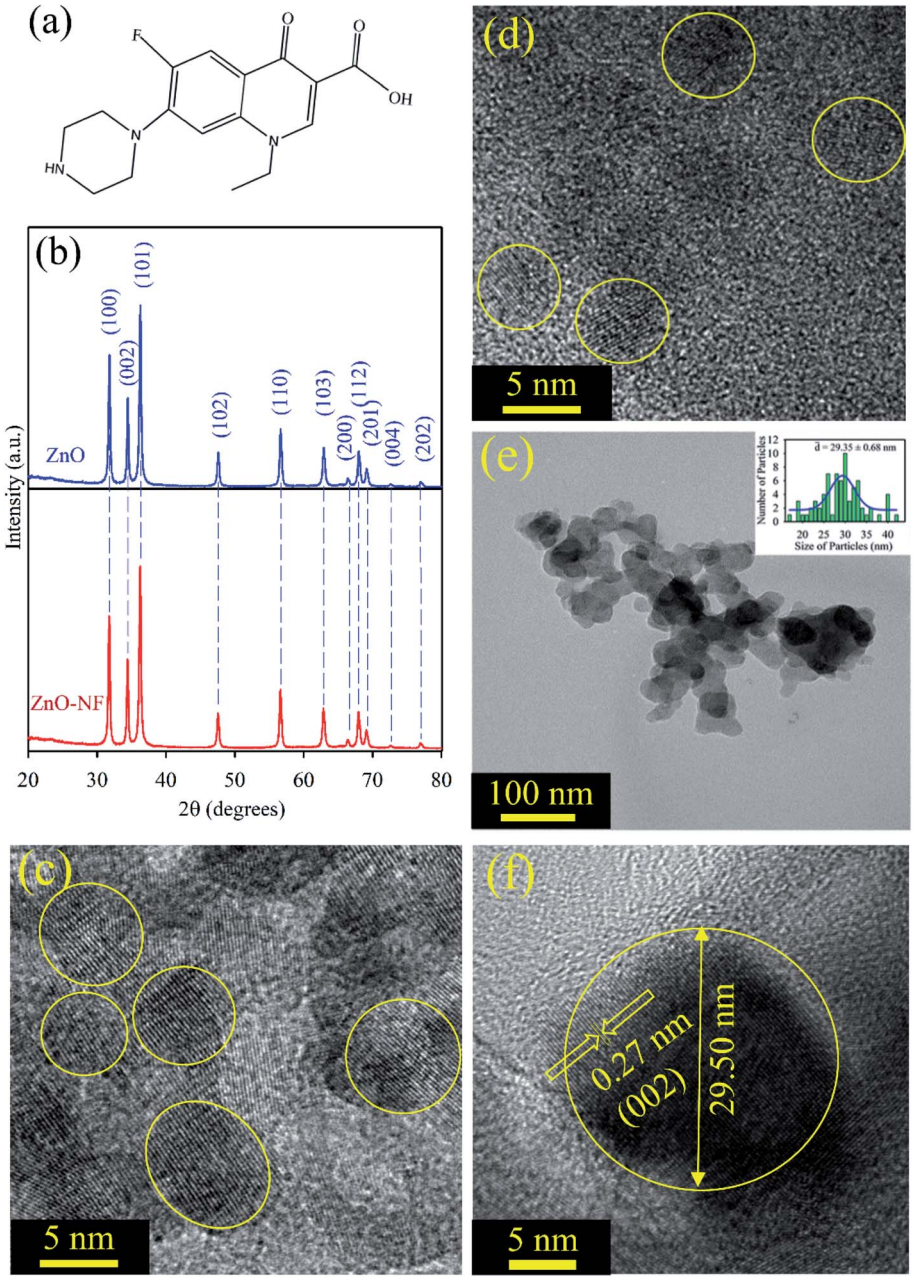

Fig. 1 (a) Depiction of the structure of norfloxacin. (b) XRD patterns of ZnO nanoparticles (Blue), and XRD patterns of ZnO–NF nanohybrid (Red). (c) The HRTEM image of ~5 nm ZnO nanoparticles. (d) The HRTEM image of ~5 nm ZnO–NF nanohybrids. (e) The TEM image of 30 nm ZnO nanohybrid, and the inset shows the particle distributions of the nanohybrid (average particle size is 29.35 ± 0.68 nm). (f) The HRTEM image of the 30 nm ZnO–NF nanohybrid.

NH and ~30 nm ZnO–NF NH were analyzed by TEM and HRTEM techniques. Fig. 1(c) illustrates the HRTEM image of the size ~5 nm ZnO NPs, and Fig. 1(d) depicts the HRTEM image of the synthesized ~5 nm NF-functionalized ZnO NH. This shows the high crystallinity nature of the synthesized ~5 nm ZnO NP and ~5 nm ZnO NH. The TEM image (Fig. 1(e)) of NH shows a sphere-like structure. The overall particle size distribution of NH is shown in the inset of Fig. 1(e), and the average particle size was found to be 29.35 ± 0.68 nm. The interplanar distance in the lattice fringe was found to be 0.27 nm of a single NH, which relates to the distance between two (002) planes, as shown in Fig. 1(f). This shows that the synthesized NH is polycrystalline in nature.[32]

4.2. Spectroscopic characterization

To investigate the optical properties of the systems, UV-Vis absorption spectra were measured for all samples. Fig. 2(a) shows the UV-Vis absorption spectra of NF (Green) and 5 nm ZnO NP (Blue) in ethanol solvent, exhibiting the characteristic peaks at 330 nm and 353 nm, respectively. After binding 5 nm

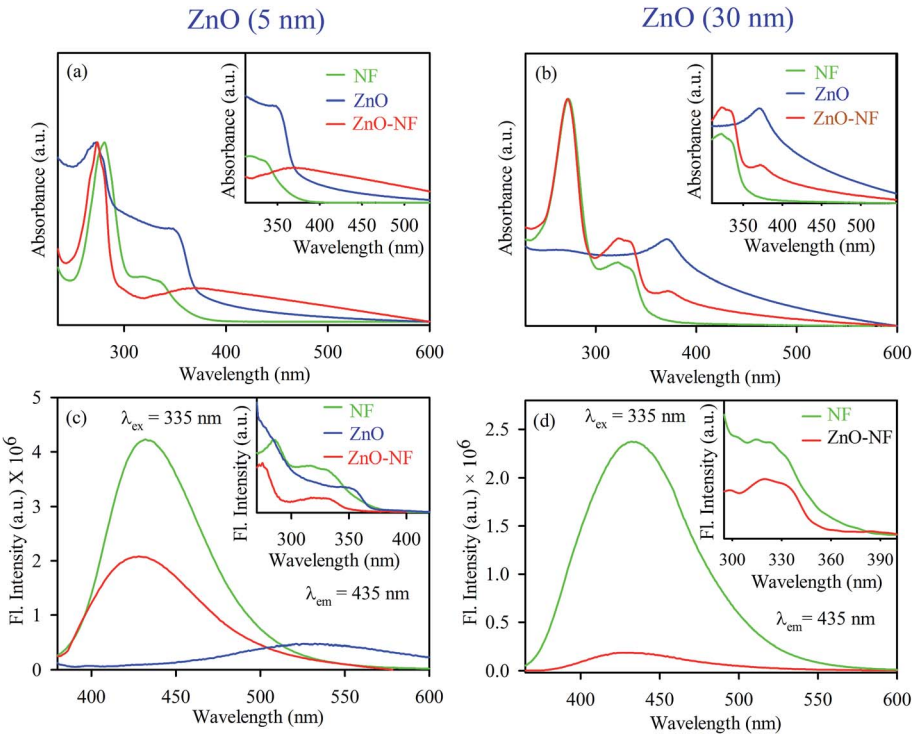

Fig. 2 (a) UV-Visible absorbance of 5 nm ZnO NP (Blue), NF (Green) and 5 nm ZnO–NF nanohybrid (Red). (b) UV-Visible absorbance of 30 nm ZnO NP (Blue), NF (Green) and 30 nm ZnO–NF nanohybrid (Red). (c) Room-temperature PL spectra (excitation at 335 nm) of NF (Green), 5 nm ZnO NP (Blue) and 5 nm ZnO–NF nanohybrid (Red). (d) Room-temperature PL spectra (excitation at 335 nm) of NF (Green) and 30 nm ZnO–NF nanohybrid (Red).

ZnO NP to NF, the characteristic peak of NF was seen in NH with a new peak at 348 nm, corresponding to 5 nm ZnO NP, which indicates the sign of complexation between NF and 5 nm ZnO NPs. Similarly, the absorption of NF (Green) and 30 nm ZnO NPs (Blue) in DMSO exhibited the characteristic peaks at 330 nm and 370 nm, respectively. After binding 30 nm ZnO to NF, the characteristic peak of NF was seen in NH (Red) with a new peak at 372 nm, corresponding to ZnO NP, as shown in Fig. 2(b). This also indicates the sign of complexation between NF and 30 nm ZnO NPs. The room temperature photoluminescence (PL) spectra of 5 nm ZnO NP (Blue) in Fig. 2(c) shows a large and broad green-yellow emission centered at around 530 nm, which can be attributed to the oxygen vacancy defect states (mostly present at the surface of the nanoparticles).[48] Here, NF exhibits an emission maximum at 435 nm upon excitation at 335 nm, and NH exhibits (slightly blue shift with respect to NF) emission maxima at 431 nm. The excitation spectra are presented in the inset of Fig. 2(c). On the other hand, 30 nm ZnO has no broad green-yellow room temperature emission centered at around 530 nm due to less oxygen vacancy defect states.[39] The room temperature photoluminescence spectra of NF (Green) and 30 nm ZnO–NF (Red) are shown in Fig. 2(d), and the corresponding room temperature excitation spectra are given in the inset. It is observed that both NF and NH exhibited an emission maximum at 435 nm upon excitation at 335 nm. In both cases, after attachment of NF to the ZnO NPs, the steady state emission intensity is significantly reduced. This may indicate the molecular level interactions during the synthesis process. The emission quenching in this region may be due to a nonradiative process, which is attributed to charge transfer from the NF to ZnO within the NH.[17]

To understand the electron transfer from NF to ZnO NPs, TCSPC studies were performed for all samples. The time-resolved fluorescence decay for 5 nm ZnO NPs (Black), free NF and 5 nm ZnO–NF was measured upon excitation with a 375 nm laser, and detected at a wavelength of 440 nm as shown in Fig. 3(a). The excited state time-resolved decay profile of NF was fitted with an exponential decay, and the lifetime was found to be 1.6 ns. The excited state lifetime of NF quenches in NH with respect to NF. The fitting parameter of the time-resolved fluorescence decays are depicted in Table 1. On the other hand, 30 nm ZnO has no time-resolved fluorescence decay profile due to less oxygen vacancy state. The time-resolved fluorescence decays for free NF (Green) and 30 nm ZnO–NF (Red) in the DMSO solvent were measured with a 375 nm laser, and emission has been detected at a wavelength of 440 nm, as shown in Fig. 3(b). The excited state lifetime of NF quenches in NH with respect to NF. It has been found that a faster component (50 ps) arises after attachment of NF on the surface of 30 nm ZnO NP (Table 1), as well as after the attachment of NF on the surface of 5 nm ZnO NP (Table 2). Here, the potential of energy transfer is eliminated, as there is no overlap between the NF emission and ZnO absorption spectra. Therefore, a faster component indicates the PET (photoinduced electron transfer) from the highest

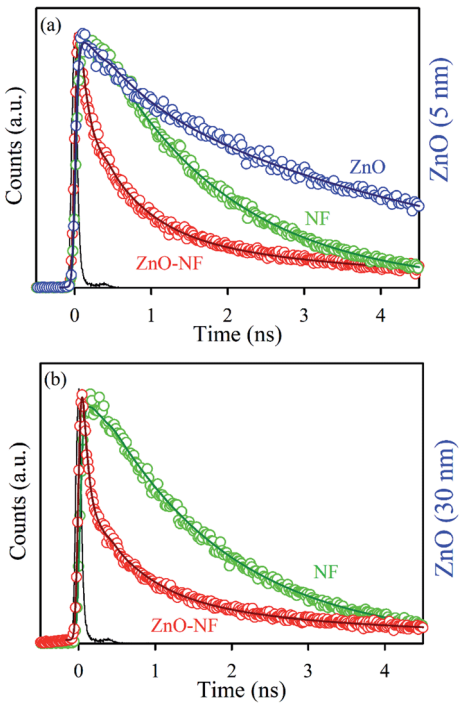

Fig. 3 (a) The picosecond-resolved fluorescence transient lifetime of 5 nm ZnO NP (Black), NF (Blue) and 5 nm ZnO–NF nanohybrid (Red). The excitation wavelength was 375 nm and the collection wavelength was 440 nm. (b) The picosecond-resolved fluorescence transient lifetime of 30 nm ZnO–NF nanohybrid (Red) and NF (Blue).

Table 1 Picosecond-resolved fluorescence transient lifetime of NF and 30 nm ZnO–NF in DMSO solvent. The emission (monitored at 440 nm) was detected with 375 nm laser excitation. The values in parentheses represent the relative weight percentages of the time components

Systems	τ_1 (ns)	τ_2 (ns)	τ_3 (ns)	τ_{avg} (ns)
NF	1.6 (100)	—	—	1.6
ZnO–NF	0.05 (70)	0.7 (22)	3.9 (8)	0.5

occupied molecular orbital (HOMO) of NF to the conduction band of the ZnO semiconductor NPs.[32] Therefore, the PET interfaced from the HOMO of NF to the CB (conduction band) of ZnO NP scale down the recombination of the electron and hole of the semiconductor. This appreciates the biological antibacterial activity,[32] which will be discussed in the later course of the discussion.

4.3. Computational study

To gain insight into the electron delocalization of the occupied and unoccupied levels of the ZnO–NF complex, we investigated the band-decomposed electron densities nature of NH. It was observed that there is a high possibility of electron transfer from NF to ZnO in the NH system, which validates the experimental findings. Among several different binding modes, the bidentate binding of NF through the carboxylic O to the Zn on

Table 2 Picosecond-resolved fluorescence transient lifetime of ZnO 5 nm, NF and 5 nm ZnO–NF in ethanol solvent. The emission (monitored at 440 nm) was detected with 375 nm laser excitation. The values in parentheses represent the relative weight percentages of the time components

Systems	τ_1 (ns)	τ_2 (ns)	τ_3 (ns)	τ_{avg} (ns)
ZnO NP	0.6 (23)	4.7 (77)	—	3.7
NF	—	0.9 (46)	2.2 (54)	1.6
ZnO–NF NH	0.08 (56)	0.6 (31)	4.1 (13)	0.7

the nonpolar [10$\bar{1}$0] surface was found to be the most energetically favorable mode of binding. The bond distances of Zn and two carboxylic O of the norfloxacin were found to be 1.98 Å and 2.01 Å, respectively, which is consistent with the computationally estimated covalent bond distances of Zn and O in ZnO (1.98 Å, 1.98 Å, 1.98 Å and 1.99 Å). This indicates the formation of covalent bonds between ZnO and NF. The binding energy of the NH has been calculated by using the formula:[49]

$$E_B = E_{NH} - E_{ZnO} - E_{NF} \quad (1)$$

The theoretically calculated binding energy of NH was found to be −1.9 eV, which indicates that the formation of the NH is energetically stable. The band decomposed charge density calculations were performed to find out the electronic distribution of the valence band maximum (VBM) and the conduction band minimum (CBM), as shown in Fig. 4(a) and (b), respectively. It suggests that in the ground state, the highest energy electrons remain localized on the O of NF. Given the energy, the electron delocalizes to the CBM of the ZnO nanoparticles. This was confirmed by time-resolved fluorescence spectroscopy with 30 nm ZnO NP. A similar result was observed for the norfloxacin complex with the $(ZnO)_{12}$ atom cluster, as shown in Fig. 4(c) and (d), which validates the experimental findings with 5 nm ZnO NP.

The DOS (density of states) analysis was continued to gain further insight into the observed effect. We calculated the TDOS (total density of states) of ZnO NPs, The gap between the VB (valence band) and CB (conduction band) of ~0.8 eV was obtained, which is in accordance with the literature data,[50,51] as shown in Fig. 5. It shows the non-magnetic and semiconducting nature. The total DOS of NF was also calculated, as shown in Fig. 5. Changes in the coordination number of atoms affect the band nature of the material, retaining the reduction in hybridization and covalent bond nature of atoms.[52] In the NH system, the contribution of the DOS near the Fermi level comes from NF. This may indicate the molecular level interactions during the formation of NH.

4.4. *In vitro* ROS and antibacterial activity

After investigation of the photoinduced electron transfer dynamics and excited state molecular dynamics, we continued our research on the antibacterial activity of NH. *In vitro* ROS generation was examined using the well-known familiar marker

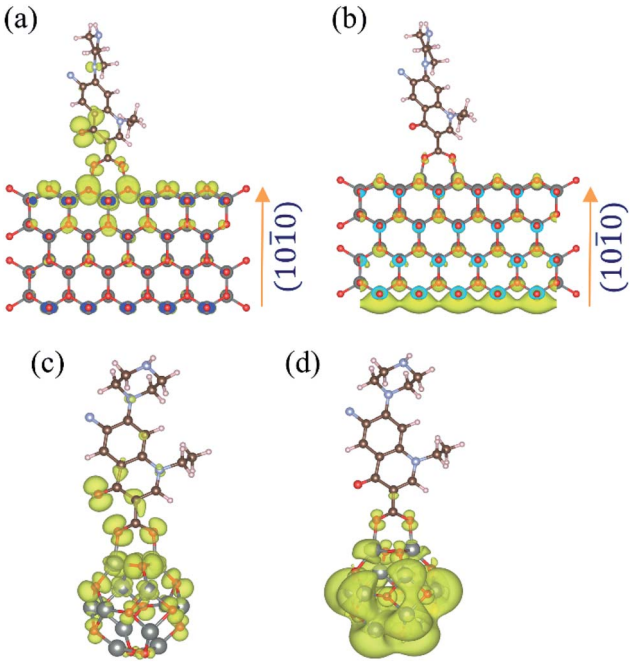

Fig. 4 Band-decomposed electron densities of ZnO–NF nanohybrids. (a) VBM of NH for the lowest energy binding conformation of NF on the nonpolar zig-zag surface of the ZnO wurtzite structure. (b) CBM of NH for the lowest energy binding conformation of NF on the nonpolar zig-zag surface of the ZnO wurtzite structure. (c) HOMO of NH for the lowest energy binding conformation of NF on the $(ZnO)_{12}$ nanocluster. (d) LUMO of NH for the lowest energy binding conformation of NF on the $(ZnO)_{12}$ nanocluster.

DCFH. DCFH is oxidized to fluorescent DCF in the presence of reactive oxygen species (ROS), and shows an emission peak near 520 nm. Thus, the enhancement of ROS during the experiment was monitored at 520 nm. The experiment was performed in the absence of light for up to 10 minutes, and under the irradiation of UV light (wavelength 375 nm) for 30 minutes. The results are depicted in Fig. 6(a). With an increase in the time of light exposure, a greater enhancement of the intensity at 520 nm was observed for the synthesized NH, as compared to NF and ZnO. Thus, the light generates efficient ROS for NH. The electron capture (from the HOMO of dye to CB of ZnO) process in NH is responsible for the enhancement of ROS generation. Mainly, this excited state electron and produced hole generate ROS from the neighboring H_2O and O_2. The detail reaction mechanisms are listed below:

$$NF + h\nu = NF\ (e^- + h^+) \quad (2a)$$

$$NF\ (h^+) + H_2O \rightarrow NF + H^+ + OH^- \quad (2b)$$

$$NF\ (h^+) + OH^- \rightarrow NF + \dot{O}H \quad (2c)$$

$$ZnO\ (e^-) + O_2 \rightarrow ZnO + \dot{O}_2^- \quad (2d)$$

$$\dot{O}_2^- + H^+ \rightarrow H\dot{O}_2^- \quad (2e)$$

$$H\dot{O}_2^- + H\dot{O}_2^- \rightarrow H_2O_2 + O_2 \quad (2f)$$

$$ZnO\ (e^-) + H_2O_2 \rightarrow ZnO + \dot{O}H + OH^- \quad (2g)$$

$$H_2O_2 + \dot{O}_2^- \rightarrow \dot{O}H + OH^- + O_2 \quad (2h)$$

For a potential application, we performed a bacterial culture *in vitro*. The bacterial culture experiment for the antibacterial activity was conducted on *E. coli*, which was incubated for around 25 hours at 37 °C with the fixed concentrations of the ZnO–NF nanohybrid, free NF and ZnO NPs as controls in the absence of light (Fig. 6(b)) and the presence (Fig. 6(c)) of light to study the cell growth rate. The enhancement of the antibacterial

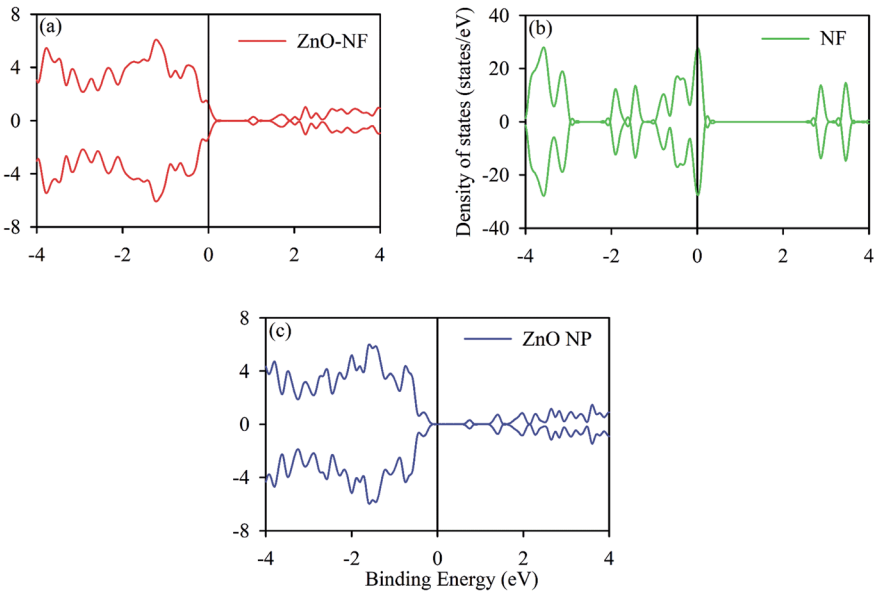

Fig. 5 (a) Density of states (DOS) of ZnO–NF. (b) DOS of NF. (c) DOS of ZnO NP surface [10$\bar{1}$0] direction. The black solid line represents the Fermi energy (E_F).

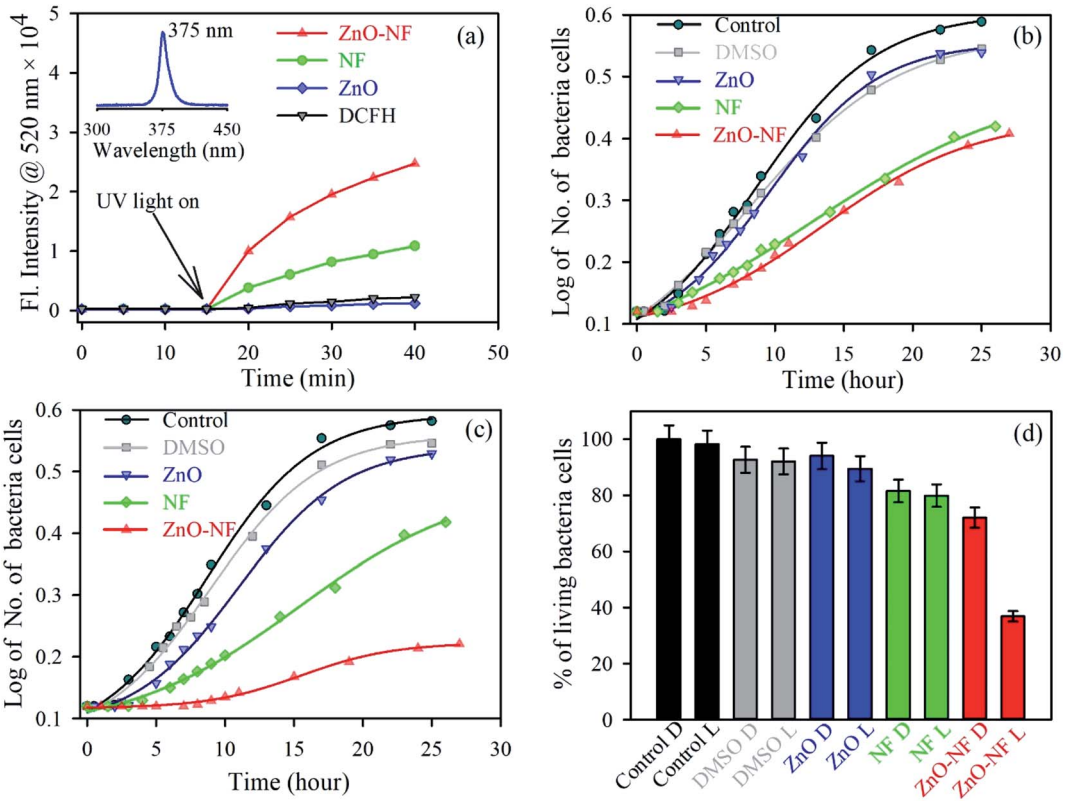

Fig. 6 (a) The DCFH oxidation with time in the presence of ZnO NP (Blue), NF (Green) and ZnO–NF nanohybrid (Red). (b) Growth of cells in the absence of UV light over time: control (Dark), DMSO (Gray), ZnO NP (Blue), NF (Green) and ZnO–NF nanohybrid (Red). (c) Growth of cells in the presence of UV light over time, control (Dark), DMSO (Gray), ZnO NP (Blue), NF (Green) and ZnO–NF nanohybrid (Red). (d) Percentage of living bacteria cells (D, Dark; L, Light).

activity was observed by the complex in the presence of light, as compared to free NF and ZnO NP. The percentages of living cells with respect to the control are shown in Fig. 6(d). NH attained a significantly higher bacteria death, which is around 65% for a particular concentration, compared to free NF (20%) and ZnO NP (11%). However, the antibacterial application depends on the dose. The bacterial death can be increased by increasing the dose concentration of ZnO–NF.[53] This approach could be applied to other antibiotics that will enhance their potential utilization in a PDT.

5. Conclusion

In summary, we investigated the enhanced antibacterial ability of ZnO–NF NH over free NF and ZnO NP using various experiments, as well as computational studies. We have established the benefit of norfloxacin (NF) as the light stimulated drug. NF was strongly associated with ZnO NPs, and the attachment was confirmed using various spectroscopy mechanisms. The excited state charge transmission process from NF to the ZnO semiconductor was confirmed by TCSPC, and supported by the first principle computational analysis. This charge transfer mechanism shows a greater extent of the ROS generations. The antibacterial photodynamic effect on *E. coli* was confirmed using the cell culture experiment, which suggests significant changes after the light stimulated drug treatment. Our results indicate that bacterial cell death occurred by a high ROS production process. It reveals that the ZnO–NF nanohybrid is much more effective in the antibacterial effect on *E. coli* cells compared to free NF and ZnO NP. This developed procedure could be applied to other antibiotics that will enhance their ability in PDT. This result provides a new path that has the capability to deliver the NF in the targeted cells, which can be used for disinfection or membrane-based antibacterial applications.

Conflicts of interest

There are no conflicts to declare.

Acknowledgements

M. N. H. and A. B. thank the CSIR (India) for providing the fellowship. T. K. M. and D. B. thank the Department of Science and Technology (DST, India) for the INSPIRE fellowship. We thank DST-SERB EMR/2016/004698 and DBT-BT/PR11534/NNT/28/766/2014 for financial support. S. K. P. thanks DST, India for the Abdul Kalam Technology Innovation National Fellowship (INAE/121/AKF).

References

1 P. Karpecki, M. R. Paterno and T. L. Comstock, *Optometry and Vision Science*, 2010, **87**, 908–919.
2 J. Jose, A. Anas, B. Jose, A. B. Puthirath, S. Athiyanathil, C. Jasmin, M. R. Anantharaman, S. Nair, C. Subrahmanyam and V. Biju, *ACS Appl. Bio Mater.*, 2019, **2**, 4681–4686.
3 M. Haque, M. Sartelli, J. McKimm and M. Abu Bakar, *Infect. Drug Resist.*, 2018, **11**, 2321–2333.
4 P. E. Sheffield and P. J. Landrigan, *Environ. Health Perspect.*, 2011, **119**, 291–298.
5 I. Chopra and M. Roberts, *Microbiol. Mol. Biol. Rev.*, 2001, **65**, 232–260.
6 C. L. Ventola, *Pharm. Ther.*, 2015, **40**, 277–283.
7 Y. Wang, Z. Zhou, J. Zhu, Y. Tang, T. D. Canady, E. Y. Chi, K. S. Schanze and D. G. Whitten, *Polymers*, 2011, **3**, 1199–1214.
8 J. Shi, A. R. Votruba, O. C. Farokhzad and R. Langer, *Nano Lett.*, 2010, **10**, 3223–3230.
9 J. Wang, P. Zhao, X. Li, H. Fu, X. Yang, G. Wang, Y. Yang, H. Wei, Z. Zhou and W. Liao, *ACS Appl. Bio Mater.*, 2020, **3**, 1580–1588.
10 R. Peng, Y. Luo, Q. Cui, J. Wang and L. Li, *ACS Appl. Bio Mater.*, 2020, **3**, 1305–1311.
11 M. R. Hamblin, *Photochem. Photobiol. Sci.*, 2018, **17**, 1515–1533.
12 X.-J. Wen, C.-G. Niu, D.-W. Huang, L. Zhang, C. Liang and G.-M. Zeng, *J. Catal.*, 2017, **355**, 73–86.
13 K. S. Kim, D. Lee, C. G. Song and P. M. Kang, *Nanomedicine*, 2015, **10**, 2709–2723.
14 A. Abdal Dayem, M. Hossain, S. Lee, K. Kim, S. Saha, G.-M. Yang, H. Choi and S.-G. Cho, *Int. J. Mol. Sci.*, 2017, **18**, 120.
15 V. Mohanraj and Y. Chen, *Trop. J. Pharm. Res.*, 2006, **5**, 561–573.
16 P. Verma and H. Pal, *J. Phys. Chem. A*, 2014, **118**, 6950–6964.
17 A. Bera, D. Bagchi and S. K. Pal, *J. Phys. Chem. A*, 2019, **123**, 7550–7557.
18 S. Sreejith, T. T. M. Huong, P. Borah and Y. Zhao, *Sci. Bull.*, 2015, **60**, 665–678.
19 C. M. Courtney, S. M. Goodman, J. A. McDaniel, N. E. Madinger, A. Chatterjee and P. Nagpal, *Nat. Mater.*, 2016, **15**, 529–534.
20 S. Wang, P. Huang and X. Chen, *ACS Nano*, 2016, **10**, 2991–2994.
21 L. Wang, C. Hu and L. Shao, *Int. J. Nanomed.*, 2017, **12**, 1227–1249.
22 S. K. Sehmi, S. Noimark, S. D. Pike, J. C. Bear, W. J. Peveler, C. K. Williams, M. S. P. Shaffer, E. Allan, I. P. Parkin and A. J. MacRobert, *ACS Omega*, 2016, **1**, 334–343.
23 Y. Jia, A. Omri, L. Krishnan and M. J. McCluskie, *Hum. Vaccines Immunother.*, 2017, **13**, 63–74.
24 G. Applerot, A. Lipovsky, R. Dror, N. Perkas, Y. Nitzan, R. Lubart and A. Gedanken, *Adv. Funct. Mater.*, 2009, **19**, 842–852.
25 R. Brayner, R. Ferrari-Iliou, N. Brivois, S. Djediat, M. F. Benedetti and F. Fiévet, *Nano Lett.*, 2006, **6**, 866–870.
26 J. Pasquet, Y. Chevalier, E. Couval, D. Bouvier, G. Noizet, C. Morlière and M.-A. Bolzinger, *Int. J. Pharm.*, 2014, **460**, 92–100.
27 K. L. Kotloff, J. P. Winickoff, B. Ivanoff, J. D. Clemens, D. L. Swerdlow, P. J. Sansonetti, G. Adak and M. Levine, *Bull. W. H. O.*, 1999, **77**, 651.
28 A. Joe, S.-H. Park, D.-J. Kim, Y.-J. Lee, K.-H. Jhee, Y. Sohn and E.-S. Jang, *J. Solid State Chem.*, 2018, **267**, 124–133.
29 Y. Wang, E. Y. Chi, D. O. Natvig, K. S. Schanze and D. G. Whitten, *ACS Appl. Mater. Interfaces*, 2013, **5**, 4555–4561.
30 M.-H. Oh, S.-H. Paek, G. W. Shin, H.-Y. Kim, G. Y. Jung and S. Oh, *J. Food Prot.*, 2009, **72**, 1262–1266.
31 A. D. Maynard, D. B. Warheit and M. A. Philbert, *Toxicol. Sci.*, 2010, **120**, S109–S129.
32 D. Bagchi, V. S. Rathnam, P. Lemmens, I. Banerjee and S. K. Pal, *ACS Omega*, 2018, **3**, 10877–10885.
33 N. Beyth, Y. Houri-Haddad, A. Domb, W. Khan and R. Hazan, *Evid. Based Complement. Alternat. Med.*, 2015, **2015**, 246012.
34 O. Rutschmann and A. Zwahlen, *Eur. J. Clin. Microbiol. Infect. Dis.*, 1995, **14**, 441–444.
35 S. P. Gopi, S. Ganguly and G. R. Desiraju, *Mol. Pharm.*, 2016, **13**, 3590–3594.
36 Z. L. Wang, *J. Phys.: Condens. Matter*, 2004, **16**, R829.
37 T. K. Maji, P. K. Sarkar, P. Kar, B. Liu, P. Lemmens, D. Karmakar and S. K. Pal, *Appl. Catal., A*, 2019, **583**, 117124.
38 F. Lu, W. Cai and Y. Zhang, *Adv. Funct. Mater.*, 2008, **18**, 1047–1056.
39 T. K. Maji, D. Bagchi, P. Kar, D. Karmakar and S. K. Pal, *J. Photochem. Photobiol., A*, 2017, **332**, 391–398.
40 S. A. Ahmed, M. N. Hasan, D. Bagchi, H. M. Altass, M. Morad, R. S. Jassas, A. M. Hameed, J. Patwari, H. Alessa, A. Alharbi and S. K. Pal, *ACS Omega*, 2020, **5**, 15666–15672.
41 S. Chaudhuri, S. Sardar, D. Bagchi, S. Dutta, S. Debnath, P. Saha, P. Lemmens and S. K. Pal, *ChemPhysChem*, 2016, **17**, 270–277.
42 S. A. Ahmed, D. Bagchi, H. A. Katouah, M. N. Hasan, H. M. Altass and S. K. Pal, *Sci. Rep.*, 2019, **9**, 19372.
43 G. Kresse and J. Hafner, *Phys. Rev. B: Condens. Matter Mater. Phys.*, 1994, **49**, 14251.
44 J. P. Perdew, K. Burke and M. Ernzerhof, *Phys. Rev. Lett.*, 1996, **77**, 3865.
45 A. Vittadini, A. Selloni, F. Rotzinger and M. Grätzel, *Phys. Rev. Lett.*, 1998, **81**, 2954.
46 P. Wisesa, K. A. McGill and T. Mueller, *Phys. Rev. B*, 2016, **93**, 155109.
47 T. K. Maji, K. Vaibhav, S. K. Pal, K. Majumdar, K. Adarsh and D. Karmakar, *Phys. Rev. B*, 2019, **99**, 115309.
48 T. Bora, K. K. Lakshman, S. Sarkar, A. Makhal, S. Sardar, S. K. Pal and J. Dutta, *Beilstein J. Nanotechnol.*, 2013, **4**, 714–725.

49 T. K. Maji, M. N. Hasan, S. Ghosh, D. Wulferding, C. Bhattacharya, P. Lemmens, D. Karmakar and S. Kumar Pal, *J. Photochem. Photobiol., A*, 2020, **397**, 112575.
50 M. Khuili, N. Fazouan, H. A. El Makarim, G. El Hallani and E. Atmani, *J. Phys. Conf. Ser.*, 2016, **758**, 012024.
51 T. K. Maji, P. Kar, H. Mandal, C. Bhattacharya, D. Karmakar and S. K. Pal, *ChemistrySelect*, 2018, **3**, 6382–6393.
52 S. D. Assa Aravindh, U. Schwingenschloegl and I. S. Roqan, *J. Chem. Phys.*, 2015, **143**, 224703.
53 M. Khatun, S. Choudhury, B. Liu, P. Lemmens, S. K. Pal and S. Mazumder, *RSC Adv.*, 2016, **6**, 105607–105617.